



A comparative study of electric current-assisted and conventional sintering of Inconel 718 superalloy

Nuri Ergin¹ · Necati Koçak¹ · Özkan Özdemir¹

Received: 17 July 2023 / Accepted: 20 February 2024 / Published online: 12 May 2024
© The Author(s) 2024

Abstract

In this study, In718 powder mixtures prepared from elemental powders following stoichiometric composition and supplied as a commercial product were produced by conventional powder metallurgy (1300 °C/4 h) and electric current-assisted sintering (ECAS)(1700-2300A/10 min) methods and followed by a double-aging heat treatment. The characterization studies determined that the best results were the sample produced by the ECAS method using the elemental powder mixture. The targeted precipitate γ' , γ'' , and δ phases were obtained after the heat treatment, and a hardness value of 344 ± 41 HV_{0.5} and a relative density of 98.96% were achieved. The sample preserved its surface integrity by exhibiting high corrosion resistance from hot corrosion studies in the temperature range of 650–850 °C and NaSO₄ + 60%V₂O₅ environment. The corrosion rate of the sample, which was subjected to electrochemical corrosion tests in 3.5% NaCl and 10% NaNO₃ solutions, was determined as 45.59 mpy and 10.56 mpy, respectively.

Keywords Superalloy · Sintering · Corrosion resistance · Electric current-assisted Sintering · Powder metallurgy

Introduction

Superalloys are Ni-, Fe- and Co-based, heat-resistant high-temperature materials, generally developed from VIII-B group elements, that exhibit high surface degradation resistance and high strength at low and high temperatures. Among these alloys, Inconel 718 is one of the alloys that is strengthened by body-centered tetragonal γ'' -Ni₃Nb and ordered face-centered cubic γ'' -Ni₃(Al, Ti) precipitates. It is also an Nb-doped Ni–Fe–Cr-based superalloy with excellent oxidation, wear and creep resistance at high temperatures, available at relatively low costs and excellent mechanical properties in the temperature range of –253 to 650 °C. These alloys are widely used in gas turbine and combustion chambers of commercial and military aircraft engines, steam turbines of electric power plants, hot work tools and casting molds of metal production processes, heat treatment equipment and chemical and petrochemical industries [1–5].

The production techniques used in obtaining the materials affect the mechanical properties of the materials, thus the quality of use and service life in service conditions. When the casting technique is chosen as the manufacturing method, problems such as macrosegregation may be encountered. In contrast, when a production method that does not allow obtaining the final product is used, a secondary process such as machining methods may be required. In recent studies, it has been emphasized that new production techniques, such as powder metallurgy, should be developed in order to eliminate the negativities in the production of superalloys [6–10]. It is thought that one of the methods that will meet these requirements is the electric current-assisted sintering (ECAS) method, which is an alternative approach to powder metallurgy.

Electric current-assisted sintering method: It is based on the principle of sintering the powders with the heat generated by the electric current by placing the cold-shaped or preforming powder mixture into the mold, applying electrical current together with mechanical pressure, in order to synthesize specific products with the desired density. When this method is compared with conventional sintering methods, it provides advantages such as faster heating speed, lower sintering temperature, faster processing time, less auxiliary sintering equipment and no need for a controlled

✉ Nuri Ergin
nergin@subu.edu.tr

¹ Department of Metallurgy and Materials Engineering,
Faculty of Technology, Sakarya University of Applied
Sciences, 54187 Sakarya, Turkey

atmosphere and cold pressing. In particular, thanks to low temperature and shorter processing time, the production of materials with fine-grain sizes close to the theoretical density and the sintering of nanosized metastable powders can be performed. In general, when conventional powder metallurgy and ECAS techniques are compared, the bonding of powder particles in the traditional powder metallurgy technique occurs under high temperature and pressure, while in the ECAS technique it occurs with electric current. Electric current accelerates the process and helps to obtain more homogeneous material. While reaching high temperatures and applying pressure in conventional powder metallurgy requires intense energy, in the ECAS technique, energy consumption is low as the sintering process is more efficient. In the ECAS technique, dense materials are obtained with the effect of electric current. This increases product quality. While the ECAS technique is partially suitable for mass production with semi-mechanized processes, conventional powder metallurgy is a method more suitable for mass production. The ECAS process is defined by names such as spark plasma sintering (SPS), field-activated sintering technique (FAST) and pulse discharge sintering (PDS) depending on parameters such as the type of current used and the way the electric current is applied. ECAS process is currently used on an industrial basis in the production of cutting tools, the production of superplastic materials requiring low temperature and pressure and the sintering of magnetic materials and medical implants [10, 11].

Marshall et al. [12] produced TCNi8 Ni-based superalloys with field-assisted sintering technology (FAST) and hot isostatic pressing techniques and compared them in terms of hardness and microstructure. They reported that they achieved better results in samples obtained with the FAST technique. They reported that this was due to the fine network of γ' precipitates produced during faster cooling rates after the FAST process [12].

In Ma et al. [13] Inconel 718 superalloy was produced with electric field-activated sintering technology (E-FAST) technique with low-voltage, high-intensity alternative current and axial pressure and reached approximately 98% relative density [13].

Shuaijiang Yan et al. [14] produced the Inconel 718 superalloy by the SPS method and obtained a high relative density and a compressive yield strength of 1349 MPa after the aging process [14].

In this study, as the starting material, the powder mixture prepared in stoichiometric composition from elemental powders to form Inconel 718 superalloy, as well as commercial

Inconel 718 superalloy powders from the market, was used. Both powder compositions were produced by conventional powder metallurgy technique and electric current-assisted sintering method. Thus, the properties of the samples produced with different techniques were compared. The samples produced by both methods were characterized with the help of metallographic examinations, density (Archimedes' principle), microhardness and corrosion tests consisting of microstructure (scanning electron microscope (SEM)) and phase analysis (X-ray patterns, EDS).

Experimental

Inconel 718 superalloy is a type of Ni–Cr–Fe-based superalloys that vary in a wide composition range and exhibit different mechanical properties depending on the composition ratio and alloying elements. The composition range of Inconel 718 superalloy is given in Table 1.

In this study, since Inconel 718 alloy will be produced by powder metallurgy method, raw material selection has been made by taking into account the effect of powder size and morphology on material properties, paying attention to meet the needs. The properties of elemental powders and commercial In718 powder used in the experiments are given in Table 2.

In the production of the samples, commercial powder, one of which is ready for sintering, was used, while the other powder mixture obtained from elemental powders by pretreatment was used. The composition was prepared in stoichiometry suitable for Inconel 718 superalloy using elemental powders, and then it was fed to the planetary ball mill at a ratio of 1:20 (powder/ball by mass) and mixed for 30 min at 600 rpm in a dry environment for a homogeneous mixture. Mechanical mixing processes were carried out with a Fritsch Planetary Mono Mill Pulverisette-6 model planetary ball mill.

Exothermic and endothermic transformation enthalpies and phase transformation temperatures were determined in order to determine the optimum production conditions of the targeted Inconel 718 superalloy. For this, DSC analyses of both powder mixtures were performed with a TA Instruments SDT-Q600 model DSC device at a heating rate of $10\text{ }^{\circ}\text{C min}^{-1}$ up to $1200\text{ }^{\circ}\text{C}$ in an argon environment.

Two different processes, conventional sintering and ECAS technique, were used in the production of the samples. The powder mixtures prepared in the production of the samples by the conventional sintering method were placed in

Table 1 Composition range of Inconel 718 superalloy [15]

| Element | Ni | Cr | Fe | Nb | Mo | Ti | Al | Other |
|---------|-------|-------|---------|----------|---------|-----------|---------|-----------|
| Mass. % | 50–55 | 17–21 | Balance | 4.75–5.5 | 2.8–3.3 | 0.65–1.15 | 0.2–0.8 | Max 2.116 |

Table 2 Properties of the starting powders used in the sintering

| Material | Purity/% | Grain size/ μm | Reference | Product code |
|------------------|----------|---------------------------|--------------------|---------------|
| Ni | 99.8 | 3–7 | Goodfellow | NI006021 |
| Fe | 99.0 | 6–8 | Goodfellow | FE006041 |
| Cr | 99.8 | 1–5 | Atlantic equipment | CAS:7440-473 |
| Co | 99.9 | 10 | Atlantic equipment | CAS:744048-4 |
| Ti | 99.5 | ≤ 40 | Alfa Aesar | CAS:7440–32-6 |
| Al | 99.0 | 7–15 | Goodfellow | AL006038 |
| Nb | 99.8 | 1–50 | Famousschem | 92.90638 |
| Mo | 99.95 | 3–7 | Alfa Aesar | CAS:7439-98-7 |
| Mn | 99.6 | < 10 | Alfa Aesar | CAS:7439-96-5 |
| Si | 99.9 | 1–5 | Alfa Aesar | CAS:7440-21-3 |
| Commercial In718 | 100 | 1–20 | Huarui Industr | HR-Inconel718 |

molds with minimized surface roughness and pressed under 150 MPa pressure to form tablets. It was then subjected to cold isostatic pressing (CIP) for 150 s under 250 MPa pressure. Isostatic pressing operations were carried out with Stansted Fluid Power brand FPG2330A-40 model CIP device. The preformed samples were sintered at 1300 °C for 4 h, and after the process, they were taken from the furnace and cooled in an open atmosphere. In the productions made using the ECAS technique, the samples were shaped with a uniaxial press under 600 MPa pressure by placing them in a mold lubricated with boron nitride and the surface roughness was minimized. The samples kept in the mold in order not to be affected by the open atmosphere were produced in 10 min in the range of 1700-3500A values. The samples produced by both methods were subjected to heat treatment consisting of a double-aging step in an argon atmosphere in order to improve their mechanical properties. The samples were heated in the oven at 980 °C, cooled in water after 1 h of waiting time, reheated to 720 °C and kept for 8 h, and then the oven temperature was cooled to 620 °C in 30 min. The formation of γ'' precipitate by keeping it at 720 °C in the first aging process and the formation of γ' precipitate by keeping it at 620 °C in the second aging process were aimed.

The characterization processes of the samples produced and heat treated were determined by density, hardness, microstructure studies, phase analyses and corrosion studies. Density measurements of the samples were made in distilled water environment on the RADWAG AS 60/220. R2 density measuring device using the Archimedes' principle. RIGAKU D MAX 2200 PC X-ray diffractometer was used to determine the phase analyses of the samples. JOEL JSM-6600 scanning electron microscope (SEM) was used to examine the morphology of the materials. Elemental changes were detected by taking point EDS analyses from phases observed in different morphologies. IXRF 500 EDS device, working synchronously with the SEM device, was used for X-ray spectrometry analyses. Hardness measurements of metallographically prepared samples before and

after heat treatment, FUTURE TECH, were carried out by applying a load of 500 g N for 10 s using a Vickers hardness tip on the FM 700 microhardness device. Hardness values were determined by taking the average of 6 separate measurements. In order to determine the hot corrosion behavior of In718 samples, which are defined as high-temperature materials, a corrosive salt environment of 40% Na_2SO_4 + 60% V_2O_5 by mass was prepared by simulating the service conditions of gas turbine engines. The samples produced by two different methods using two different starting powders and subjected to double-aging heat treatment were embedded in this salt mixture and kept at temperatures of 650 °C, 750 °C and 850 °C for 1, 3, 5, 10, 20 and 30 h. then cooled to room temperature. After isothermal hot corrosion studies, the samples were washed with pure water and dried to remove salt residues deposited on the sample surface. The corrosion rate was calculated from the mass loss by considering the ratio of the mass change of the samples to the surface area. Mass changes of the samples were determined by an electronic balance with a sensitivity of 0.00001 g. Electrochemical corrosion experiments were carried out at room temperature on the Gamry computer-controlled potentiostat/galvanostat test device using the potentiodynamic polarization technique. In the experiments carried out according to the three-electrode technique in the glass corrosion cell, saturated Ag/AgCl was used as the reference electrode and graphite was used as the reference electrode. An area of 0.785 cm^2 of the produced samples was corroded. During corrosion tests, two different solution environments were used as solutions: 3.5% NaCl and 10% NaNO_3 .

Experimental results

In order to determine the shape of the powder mixtures used in the sample production and to determine the oxide content of the particles that are likely to be oxidized due to the size of the surface area, SEM–EDS analyses were

performed and the initial powder properties were determined before production. SEM–EDS analyses of the mixture obtained from elemental powders are given in Fig. 1 and the commercial powder mixture in Fig. 2. In the detailed examinations, it was determined that the desired stoichiometric composition was obtained in the mixture prepared from elemental powders, there was agglomeration and it contained 6.3% oxygen by mass. One result of the production of commercial Inconel 718 powder by gas atomization method, it was determined that it is in spherical form and contains approximately 2% oxygen by mass.

In the powder metallurgy technique, the particle size distribution of the powders affects the density and flow properties of the samples, thus determining the amount of pores and mechanical properties. The particle size distribution of the commercial powder and elemental powder

mixture used as raw material for producing Inconel 718 superalloy is given in Fig. 3a, b.

From the particle size distribution analysis of commercial In718 powders, it was determined that the average particle size was 74 μm and ranged between 57.02–118.6 μm , while the average particle size of the elemental powder mixture was 53 μm and ranged between 8.19–111.1 μm . The particle size distribution of the elemental powder mixture is in a wider range than the commercial In718 alloy powders, which is thought to be due to the agglomeration that occurs during the mixing process in the planetary mill and the particles that break off in different sizes with the impact of high-speed impact.

DSC analysis is generally accepted as a key technique in phase transformation studies, and phase transformations can be detected by endothermic or exothermic peaks [16]. In the production of Inconel 718 samples with two

Fig. 1 SEM–EDS analysis of mechanically mixed Inconel 718 powder

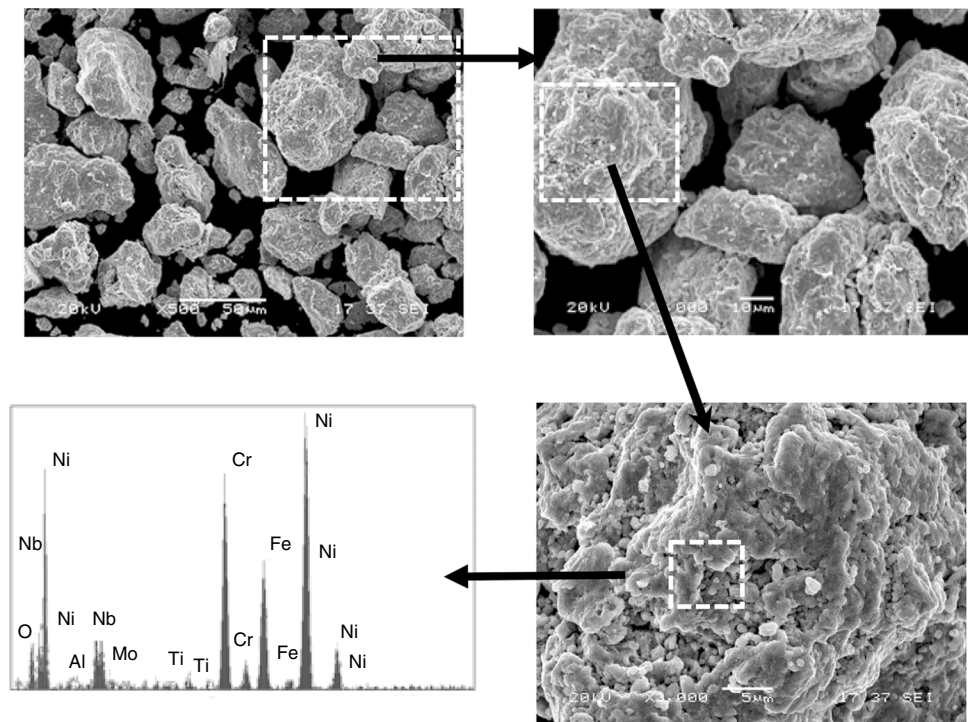
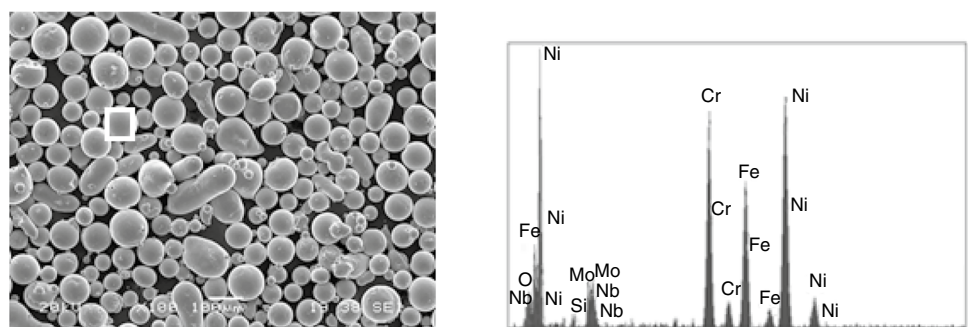


Fig. 2 SEM–EDS analysis of commercial Inconel 718 powder



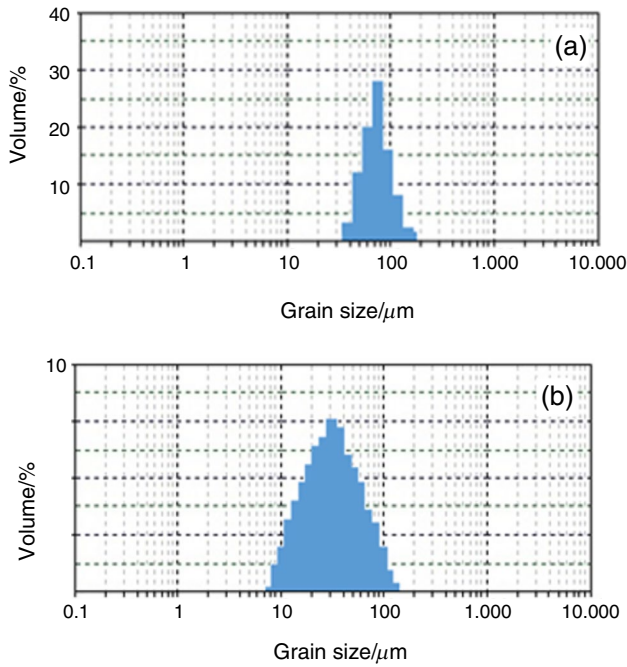


Fig. 3 Powder size distribution of In718 starting powders **a** commercial **b** mixed elemental

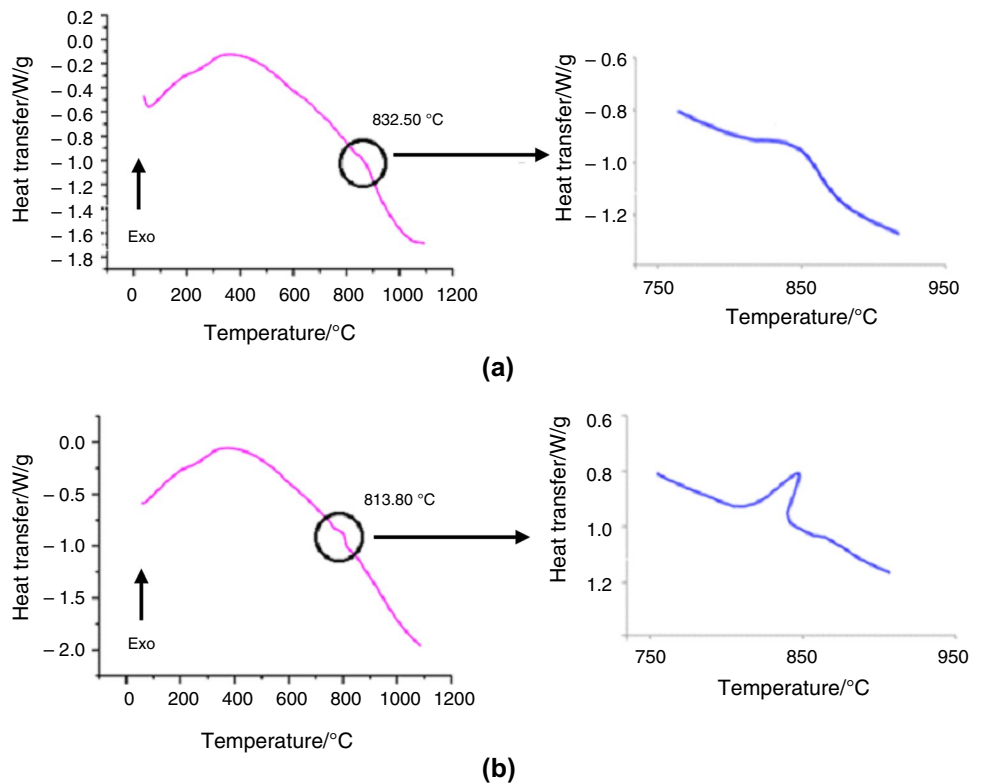
different methods using two different powder sources, DSC analysis was performed to determine the temperature for the conventional sintering method and to determine the

exothermic reaction temperature for the ECAS method, and the results are given in Fig. 4a, b.

Faheem et al. [16] reported that the Inconel 718 superalloy had an exothermic reaction at temperatures of 869 °C and 901 °C in their DSC analysis studies performed at two different holding time heat treatment temperatures and for two different holding times. Mei et al. [17] in their DSC analysis of cold rolled Inconel 718 superalloy, reported that γ'' -precipitate formed at 804 °C and δ -precipitate at 928 °C. In this study, in the DSC analyses of two different powders to be used in the production of Inconel 718, exothermic peaks were detected at 832.5 °C in commercial powder and 813.8 °C in elemental mixture powder.

Morphological examinations of the samples, which were produced and heat-treated by taking into account the temperatures determined by DSC analysis, were made with SEM analyses. Metallographic preparation of superalloys is generally very difficult. The carbide layers contained in the samples cause brittle characteristics during cutting, sanding and polishing processes and easily break off during the abrasion process and cause serious damage to the material surface. In addition, depending on the corrosion resistance of superalloys, the duration of the etching process in the order of minutes causes excessive corrosion locally [18]. For this reason, microstructural examinations of the samples were made by creating broken surfaces using SEM analysis technique. SEM microstructure images of samples obtained from elemental powder

Fig. 4 DSC analysis of Inconel 718 alloy mixed powders **a** commercial **b** elemental



mixture and commercial powders by two different production methods are given in Fig. 5.

From the SEM analysis results, it is seen that the phase transformation is completed for all samples and dense microstructures with low porosities are obtained. It was observed that the sample produced by ECAS technique using elemental powder mixture had coarse grain structure, homogeneous structure and higher density compared to other samples. The sample produced by the ECAS technique using commercial powder has a similar structure, but heterogeneous distribution and relatively low density. The samples produced by the conventional PM method, on the other hand, exhibit a second grain structure similar to the rod-like appearance beside the equiaxed grain structure. From the microstructure images (Fig. 5), it was seen that the sample obtained using commercial powders was homogeneous, the sample obtained with the elemental powder mixture was denser, and the phase in the rod-like appearance was less.

SEM analysis was carried out in order to determine the precipitation phases of the produced and heat treated samples and to determine the microstructure distribution of the elements that give the material certain properties. In Fig. 6, EDS analysis of the sample produced by ECAS technique using elemental powder mixture is given. According to the EDS analysis results taken from different parts of the sample, it is seen that each region of the sample has a similar composition, the elements are homogeneously distributed in the structure, and the targeted Inconel 718 chemical composition has been reached.

EDS analysis of the sample produced by ECAS technique using commercial In718 powder is given in Fig. 7. The precipitate phase showing homogeneous distribution on the matrix is seen from the high-magnification microstructure image. It can be seen that the matrix phase (zone 1) is very close to the expected chemical composition and also contains oxygen. In region number 2, it was determined that the amount of Ni and Fe, which are the main elements that make up Inconel 718, decreased significantly, and the amounts of Al and Nb increased.

EDS analysis of both powder mixtures produced by the conventional PM method is given in Figs. 8 and 9. It was observed that the samples, which were heat treated after production, generally consisted of an equiaxed and rodlike grain structure. EDS analysis was taken from 2 different points on different grain structures. It is seen from the EDS analysis results taken from the equiaxed phase (region 1) of the sample obtained with the elemental powder mixture using the conventional PM method that it has a composition close to the sample produced with ECAS. According to the results obtained from phase 2, which is the rod-like appearance, it was determined that the amount of Ni increased while the amount of Fe decreased considerably. It is seen that the sample produced by the conventional PM method using commercial powders is close to a similar composition, the amount of Nb and Mo is relatively low, and the amount of Fe decreases in the same way in the rodlike phase, and the amount of Cr increases. In addition, the oxygen content was not found in the samples obtained

Fig. 5 SEM micrographs from the fractured surfaces of the In 718 samples produced by **a** ECAS using elemental mixed powder, **b** PM using elemental mixed powder, **c** ECAS using commercial mixed powder, **d** PM using commercial mixed powder

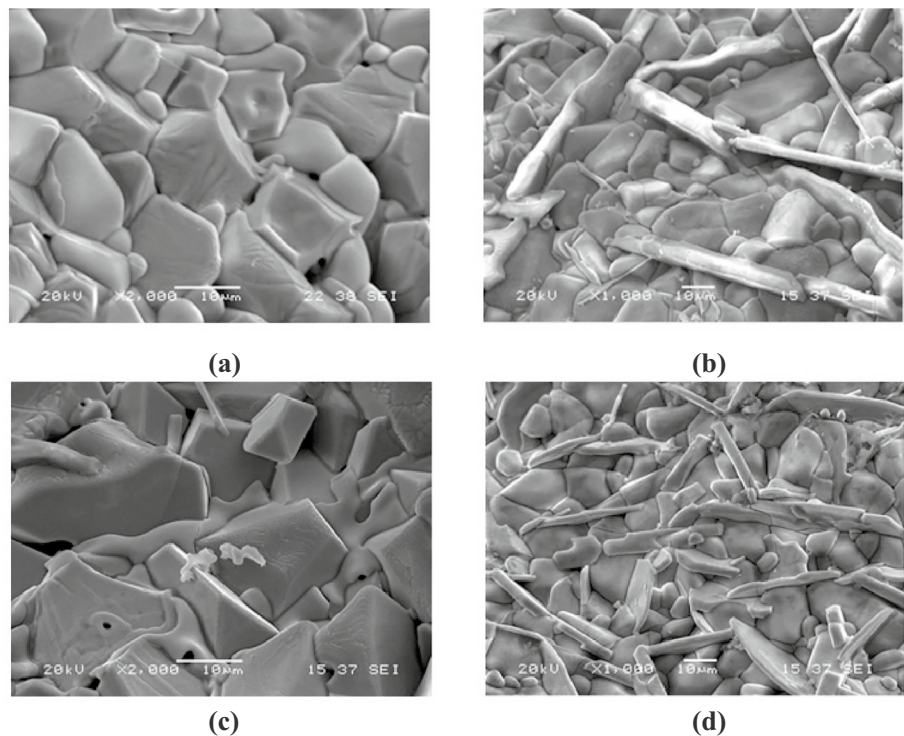


Fig. 6 EDS analysis of the In 718 sample produced by ECAS technique using an elemental powder mixture

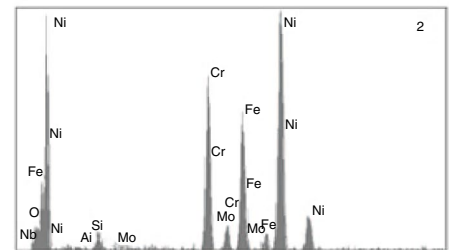
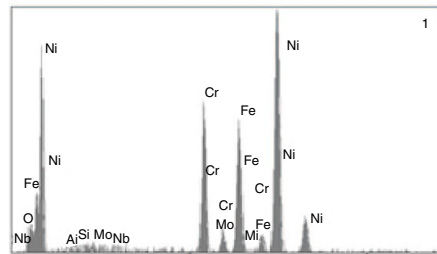
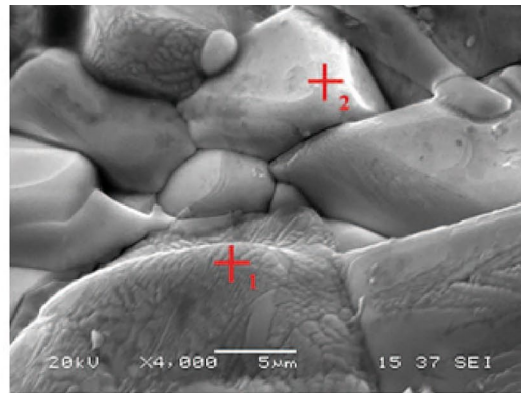
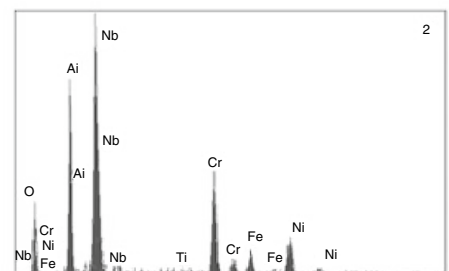
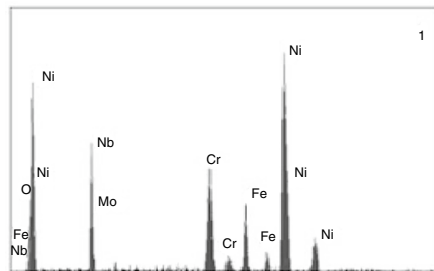
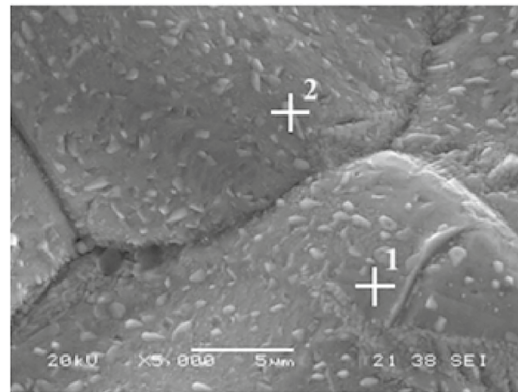


Fig. 7 EDS analysis of the In 718 sample produced by ECAS technique using commercial powders



with conventional PM. Zhu et al. [19] interpreted the rod-like structure of the samples produced by the conventional PM method as columnar dendrites and emphasized that it was due to temperature gradients during the solidification

process. Considering that the preferred temperature in the conventional PM method is close to the melting temperature of these materials, it is thought to be a similar situation.

Fig. 8 EDS analysis of the sample produced by conventional PM method using elemental powder mixture

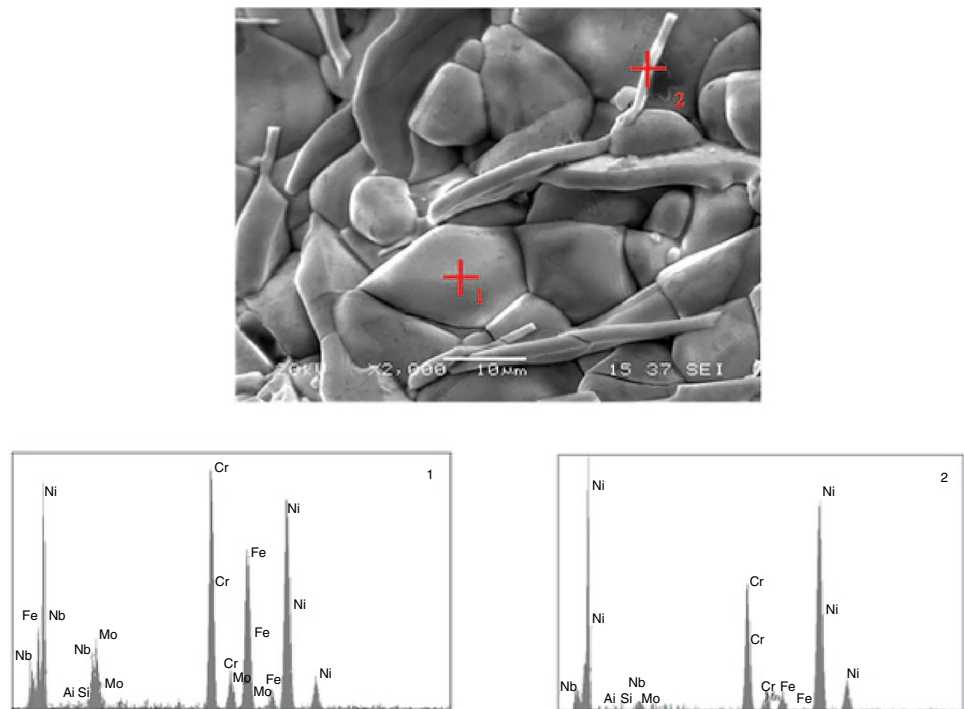
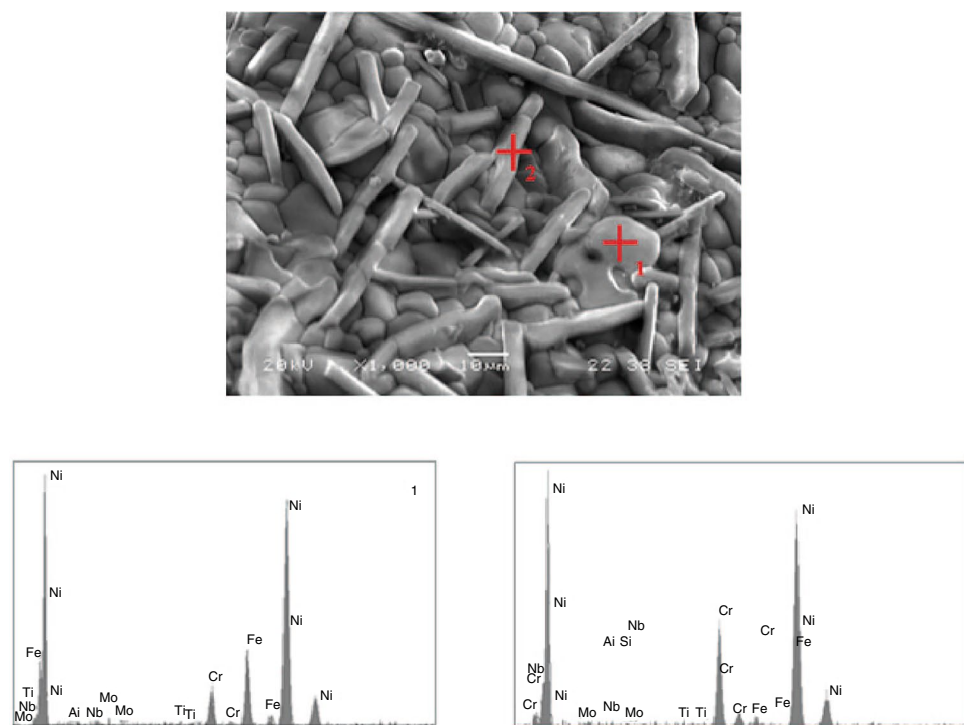


Fig. 9 EDS analysis of the sample produced by the conventional PM method using commercial In718



X-ray diffraction method was used to detect the phases formed in Inconel 718 superalloys, produced under similar conditions with ECAS and conventional PM methods, using a homogeneous mixture prepared from elemental powders and commercial In718 powders and heat treated.

XRD diffraction analyses of sintered Inconel 718 superalloy are given in Fig. 10.

It was determined that the peaks of the Inconel 718 gamma (γ) matrix were obtained in the XRD patterns of the samples after production. In both production methods

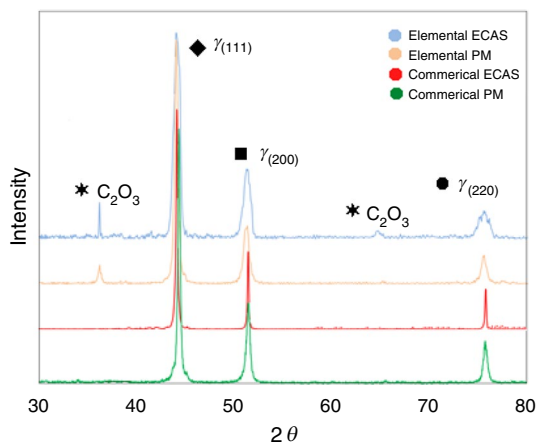


Fig. 10 XRD diffraction analyses of sintered Inconel 718 superalloy

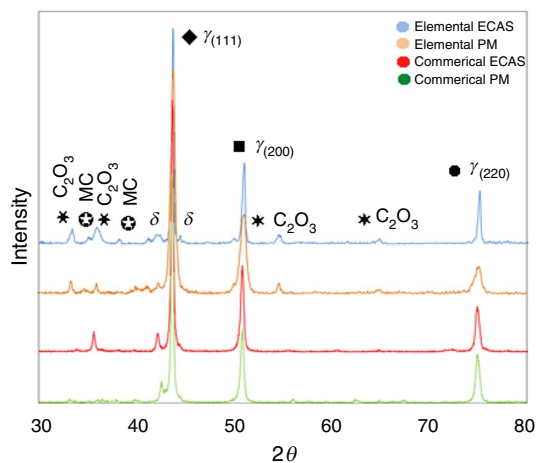


Fig. 11 XRD diffraction analysis of Inconel 718 superalloy after heat treatment

using elemental powder mixture, the presence of the C_2O_3 peak was determined as well as the matrix phase. While the oxygen content of the elemental powder mixture was 6.3% in SEM–EDS analysis, it was found to be approximately 2% in Commercial In718. For this reason, it is thought that the C_2O_3 peak occurs due to the high oxygen content in the productions using an elemental powder mixture. No C_2O_3 peak was found in the samples made at the end of a similar production process using commercial In718 powder.

δ , MC and C_2O_3 phases were determined in the XRD patterns after the double-aging process to improve the mechanical and high-temperature properties such as strength and hardness of the produced samples. XRD diffraction analysis of Inconel 718 superalloy after heat treatment is given in Fig. 11.

While the precipitate phases defined in the literature were reached in the samples produced by both methods using

elemental powders, the MC phase could not be detected in the production made with ECAS using commercial powder, and the precipitates were determined with low peak intensity in the sample produced with conventional PM. In literature reviews, it has been reported that while δ and NbC precipitate phases are easily detected after heat treatment in some studies [20, 21], it is difficult to detect precipitate phases by X-ray in some studies [22]. However, it is stated that the presence of precipitates can be indirectly determined by changes in the patterns of the matrix phase [23].

Cr and Ni in Inconel 718 superalloy; γ matrix phase with a face-centered cubic crystal lattice structure, Nb; The γ'' (Ni_3Nb) main precipitate phase with body-centered tetragonal crystal structure dispersed in the γ matrix and Ti and Al form the γ' phase, which is $Ni_3(Al, Ti)$ intermetallic precipitate with face-centered cubic structure. The orthorhombic δ phase and MC type carbides (M mostly Nb, Ti) precipitated at the grain boundaries improve the creep properties of Inconel 718. Also, Al and Cr; Al_2O_3 and Cr_2O_3 form a protective layer on the surface in the form of oxide films [24, 25]. It is reported that γ'' precipitate will be formed in the first aging step at 720 °C of double-aging heat treatment applied to Inconel 718 superalloy, and γ' precipitate will be formed in the second aging process at 620 °C [26]. Since the γ'' and γ' phase peaks have values very close to the diffraction peak of the γ phase [20], they are very difficult to detect in XRD patterns after heat treatment. While the lattice parameter of the γ'' phase in the DO_{22} (regular tetragonal, Pearson symbol; tI8) structure is $a=0.3624$ and $c=0.7406$ nm, the lattice parameter of the γ' phase in the L12 (regular YMK, Pearson symbol; cP4) structure is $a=0.3690$ nm. The diffraction plane, interplanetary distance, diffraction angle and relative density of the γ' and γ'' phases are given in Table 3.

Since the precipitate phases formed after the heat treatment cannot be easily detected in the XRD patterns of the superalloys produced and heat treated, the mechanical properties of the samples after the heat treatment are examined or DSC analyses are performed [27, 28]. In the present study, DSC analysis was performed on the samples obtained by using two different production methods and two different powders, and it was determined whether a precipitate phase was formed or not. DSC analyses taken from the produced samples after heat treatment are given in Fig. 12. From the DSC analysis results, it is seen that the precipitate phases are formed in the samples at very close temperatures.

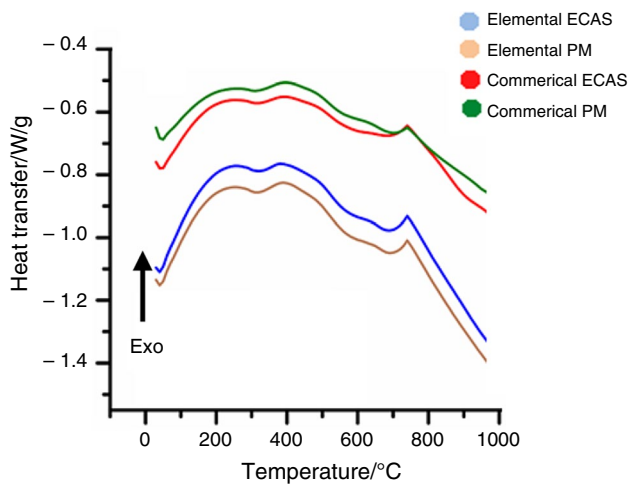
The relative densities of the samples produced and heat treated were determined according to the Archimedes' principle and are given in Table 4.

The relative densities of the samples produced with elemental powders were over 98%, and it was determined that the most concentrated sample in this group was the sample obtained with ECAS (98.96%). The commercial powder is in

Table 3 Diffraction plane (*hkl*), interplanar distance (*d*), diffraction angle (2θ) and relative density (*I*) of γ' and γ'' phases [20]

| γ'' phase | | | | γ' phase | | | |
|------------------|----------|-----------|----------|-----------------|----------|-----------|----------|
| <i>hkl</i> | <i>d</i> | 2θ | <i>I</i> | <i>hkl</i> | <i>d</i> | 2θ | <i>P</i> |
| 101 | 3.262 | 27.34 | 5 | 100 | 3.600 | 24.73 | W |
| 110 | 2.561 | 35.04 | 1 | 110 | 2.546 | 35.26 | W |
| 112 | 2.107 | 42.92 | 100 | 111 | 2.079 | 43.54 | VS |
| 103 | 2.040 | 44.41 | – | 200 | 1.800 | 50.72 | S |
| 004 | 1.852 | 49.20 | 16 | 210 | 1.610 | 57.22 | VW |
| 200 | 1.812 | 50.36 | 31 | 211 | 1.470 | 63.28 | VW |
| 202 | 1.627 | 56.57 | 1 | 220 | 1.273 | 74.56 | S |
| 211 | 1.587 | 58.13 | 1 | 300 | 1.200 | 79.95 | VW |
| 204 | 1.294 | 73.13 | 18 | 310 | 1.138 | 85.25 | VW |

VS very strong, S strong, W weak, VW very weak

**Fig. 12** DSC analyses of the produced samples after heat treatment**Table 4** Calculated densities of the samples

| Material | Density/g cm ⁻³ | Theoretical density/g cm ⁻³ | Relative density/% |
|-----------------|----------------------------|--|--------------------|
| Elemental ECAS | 8.106 | 8.192 | 98.96 |
| Elemental PM | 8.065 | | 98.46 |
| Commercial ECAS | 8.050 | 8.220 | 97.94 |
| Commercial PM | 8.025 | | 97.63 |

a narrow range (57.02–118.6 μm) and generally in spherical form, while the elemental powders that make up the mixture are amorphous and sharp-edged, with a wide grain size range (8.19–111.1 μm). It is thought that the relative densities of the samples produced using elemental powder are higher than the samples produced with commercial In718 powder, due to the wide size distribution of the elemental powders and the additional exothermic reaction temperature released. Although there is agglomeration after the mixing process applied in the planetary mill, it maintains

Table 5 Hardness values of the samples

| Material | The sample ($\text{HV}_{0.5}$) | After heat treatment ($\text{HV}_{0.5}$) |
|-----------------|----------------------------------|--|
| Elemental ECAS | 245 \pm 13 | 344 \pm 41 |
| Elemental PM | 214 \pm 17 | 331 \pm 32 |
| Commercial ECAS | 208 \pm 11 | 314 \pm 11 |
| Commercial PM | 200 \pm 6 | 285 \pm 17 |

its irregular shape. Although this situation seems to be a disadvantage compared to commercial powder, it is known that complex shaped powders have more ability to form bonding points after pressing and are effective in breaking the oxide layer that may form on the surface of neighboring particles with its sharp-edged structure [29].

Determining the hardness values of the samples is very important in terms of giving information about their mechanical properties. The hardness measurements of the samples before and after the heat treatment were made using the Vickers hardness tip in the microhardness device and the hardness values found are given in Table 5. While the hardness values of all samples produced before the heat treatment were in the range of 200–245 $\text{HV}_{0.5}$, it was determined that it changed between 285–344 $\text{HV}_{0.5}$ after the heat treatment. It was observed that the hardness values increased in parallel with the increase in relative density. It was determined that the intensity of the precipitate phase peaks in the XRD pattern of the samples produced by the ECAS method using the elemental powder mixture, after double-aging heat treatment, was higher than the other samples and these samples had the highest hardness and density values.

It is known that the hardness of Inconel 718 superalloy, produced in a wide composition range, varies in the range of 30–40 HRC (285–388 HV) depending on the applied aging heat treatment temperature and time. Qin et al. [30] reported the hardness values obtained from 3 different regions of

Inconel 718 superalloy obtained by using vacuum injection melting, electro slag melting and vacuum arc melting techniques after heat treatment as 37.3 HRC, 41.67 HRC and 44.2 HRC. Tucho et al. [31] reported that the hardness values of the samples they produced by selective laser melting were in the range of 207–304 HV, depending on the heat treatment temperature and duration. The corrosion properties of the produced and heat-treated samples were determined by the time-dependent mass changes of the samples exposed to the hot corrosion environment and by extrapolation to the corrosion potential of the Tafel zones electrochemically. Inconel 718 superalloys find wide use in gas turbine engines as “Low Cost High-temperature Construction Materials” [32, 33]. Gas turbine engines are exposed to hot corrosion damage as a result of the formation of Na_2SO_4 and V_2O_5 salts that melt at low temperatures (950 °C) of impurities such as Na, S and V in their fuels. In this study, mass % 40 Na_2SO_4 + 60% V_2O_5 mixed corrosive salt environment was prepared by simulating the service conditions of gas turbine engines in order to determine the hot corrosion behavior of In718 samples, which is defined as a high-temperature material. The samples, which were produced with two different methods using two different initial powders and carried out double-aging heat treatment, were buried in this salt mixture and kept at temperatures of 650 °C, 750 °C and 850 °C for 1, 3, 5, 10, 20 and 30 h. In this way, the corrosion rate was determined from the mass change with isothermal hot corrosion studies.

In Fig. 13, mass changes of samples produced by ECAS method using commercial In718 powders are given depending on temperature and time. It is seen that the mass change of the samples increases with the increase in temperature and time. At the end of the sample's 30-h isothermal hot

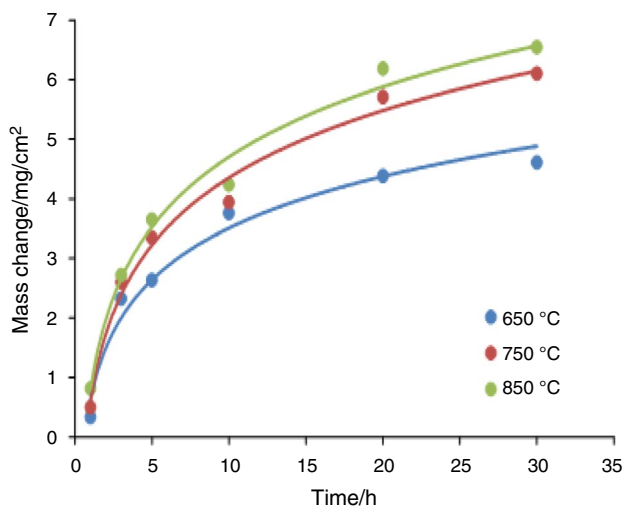


Fig. 13 Mass changes of commercial In718 samples produced with ECAS technique depending on time and temperature

corrosion experiments, the mass changes at 650, 750 and 850 °C temperatures were determined as approximately 4.5, 6 and 6.5 mg/cm^2 , respectively.

The mass changes of the samples produced by the conventional PM method using commercial In718 powders, depending on temperature and time, are given in Fig. 14. It is observed that there is no spalling in the samples exposed to hot corrosion at temperatures of 650 °C and 750 °C. However, while an increase in mass was observed in the sample exposed to hot corrosion at 850 °C until the 10th hour, it was observed that after the 10th hour, with the spallage of the layers formed on the surface as a result of corrosion, a serious decrease in mass occurred.

The mass changes of the samples produced with the ECAS method and conventional PM technique using the elemental powder mixture, depending on the temperature and time, are given in Figs. 15 and 16. It was observed that

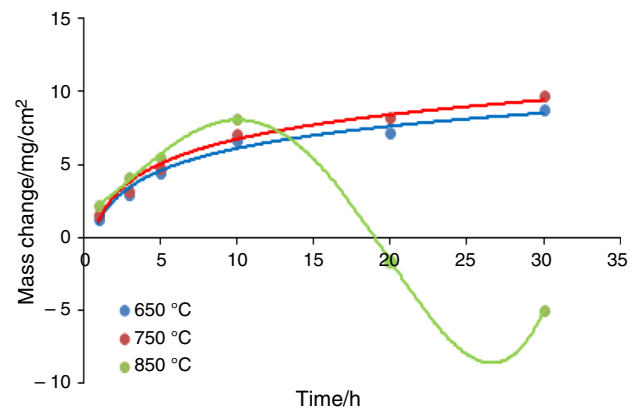


Fig. 14 Mass changes of commercial In718 samples produced with conventional PM depending on time and temperature

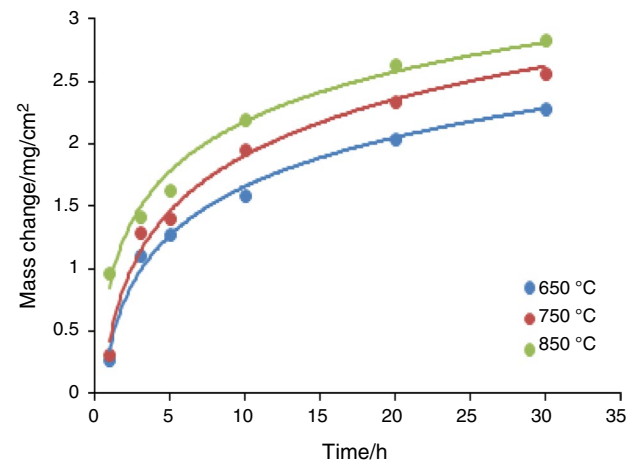


Fig. 15 Mass changes of elemental In718 samples produced by ECAS technique depending on time and temperature

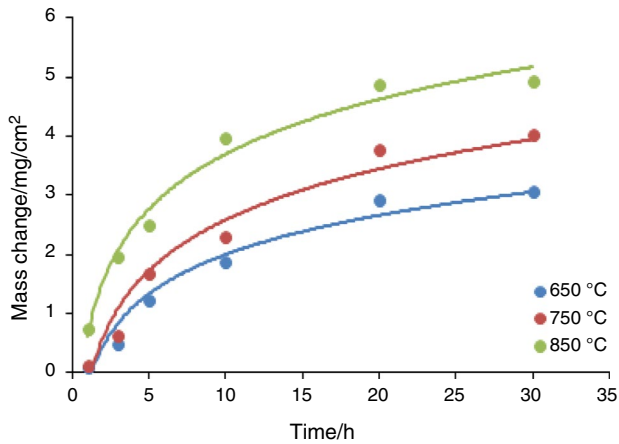


Fig. 16 Mass changes of elemental In718 samples produced by conventional sintering technique depending on time and temperature

the mass change curves for both groups of samples changed in accordance with the parabolic change with the increase in temperature and time.

The hot corrosion behavior of the samples produced using two different production methods and two different powder mixtures at constant temperatures of 650, 750 and 850 °C, depending on the time, were compared. While the mass change of the samples produced by the ECAS method using the elemental powder mixture was the least at all test temperatures, the mass change of the samples produced by the conventional PM method from commercial powders was determined to be the highest at 650 and 750 °C. In addition, when the hot corrosion temperature for this material is increased to 850 °C, it has been observed that the layer thicknesses formed on the surface at the end of the test period of 10 h and its mass decreases significantly with the spalling. Calculations for the commercial PM sample are based on a corrosion time of 10 h.

In order to determine the hot corrosion behavior of the samples, parabolic rate constant (k_p) values were calculated

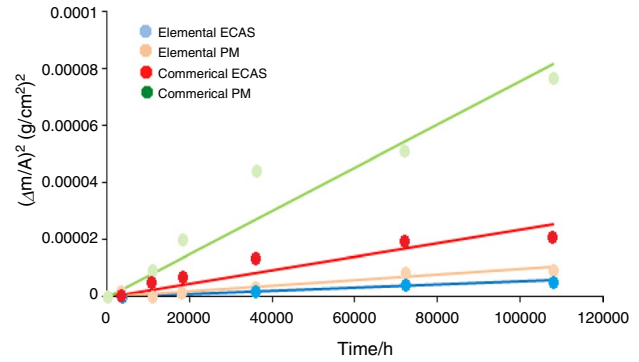


Fig. 17 Parabolic rate constants (k_p) of samples hot corroded at 650 °C

and given in Table 6. It is known that there is an inverse relationship between the parabolic rate constant and the corrosion behavior of the material. Therefore, among the samples exposed to hot corrosion at 650, 750 and 850 °C, the commercial In718 PM sample had the worst corrosion behavior, while the elemental Inconel 718 ECAS sample had the best corrosion behavior. Figures 17–19 show parabolic rate constants (k_p) of hot worn samples at 650 °C, parabolic rate constants (k_p) of hot worn samples at 750 °C and 850 °C rate constants of hot worn samples (k_p) parabolic rate constants.

Kamal et al. [34] investigated the hot corrosion behavior of Superfer 800H superalloy in $\text{Na}_2\text{SO}_4 + 60\% \text{V}_2\text{O}_5$ hot salt solution at 900 °C and determined k_p values as 1.684 after 10 cycles, 2.931 after 20 cycles and 2.437 $\text{g}^2\text{cm}^{-4}\text{s}^2$ after 35 cycles. The elements that make up the chemical composition of Superfer 800H superalloy are similar to those of Inconel 718 superalloy and the amount of Cr it contains is the same, and it does not contain Nb and Mo alloying elements. It is known that the main element providing the hot corrosion resistance of superalloys is Cr, but Ti, Al and Nb elements play an important role in increasing the hot corrosion resistance [35]. Therefore, it is thought that the reason why the corrosion resistance obtained in this study is higher

Table 6 Calculated parabolic rate constant (k_p) values of the samples

| Material | 650 °C | | 750 °C | | 850 °C | |
|----------------------------|--------|-------|--------|-------|--------|-------|
| | k_p | R^2 | k_p | R^2 | k_p | R^2 |
| Elemental Inconel 718 ECAS | 0.52 | 0.96 | 0.61 | 0.93 | 0.76 | 0.93 |
| Elemental Inconel 718 PM | 1.06 | 0.96 | 1.61 | 0.96 | 2.33 | 0.89 |
| Commercial In718 ECAS | 2.23 | 0.89 | 3.72 | 0.95 | 4.97 | 0.95 |
| Commercial In718 PM | 7.02 | 0.94 | 9.57 | 0.94 | 6.56 | 0.99 |

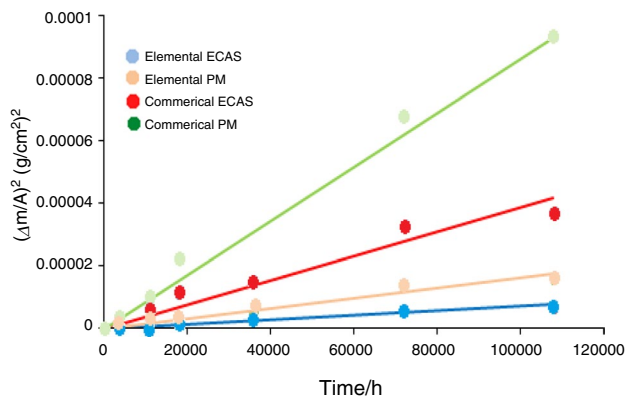


Fig. 18 Parabolic rate constants (k_p) of samples hot corroded at 750 °C

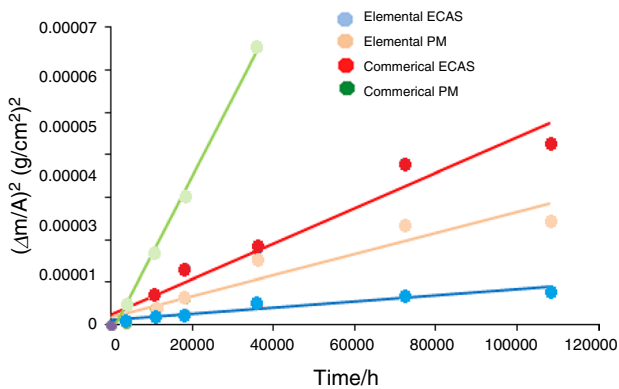


Fig. 19 Parabolic rate constants (k_p) of samples hot corroded at 850 °C

compared to the Superfer 800H superalloy is the Nb content it contains.

Studies in recent years indicate that the hot corrosion resistance of materials designed for use in gas turbines can be increased by improving the surface properties of especially superalloys with coatings [36]. Kamal et al. [37] in their study on the hot corrosion behavior of Cr_3C_2 NiCr coated and uncoated Superni 718 superalloy with D-gun thermal spray process in $Na_2SO_4 + 60V_2O_5$ hot salt solution at 900 °C, when the ratio of time dependent mass change to surface area is examined, the sample becomes parabolic up to 25 cycles. However, after 25 cycles, a rapid decrease in mass was observed. It has been determined that the same material exhibits good corrosion resistance up to 50 cycles after Cr_3C_2 -NiCr coating process and then loses its properties. When the k_p values were examined, it was determined

Table 7 Tafel analysis results of samples in 3.5% NaCl solution

| Material | E_{corr}/mV | $I_{corr}/mA\ cm^{-2}$ | Corrosion rate/mpy |
|-----------------|---------------|------------------------|--------------------|
| Elemental ECAS | -0.2838 | 1.28 | 45.59 |
| Elemental PM | -0.3112 | 1.35 | 65.93 |
| Commercial ECAS | -0.3306 | 1.47 | 76.09 |
| Commercial PM | -0.3498 | 1.52 | 77.82 |

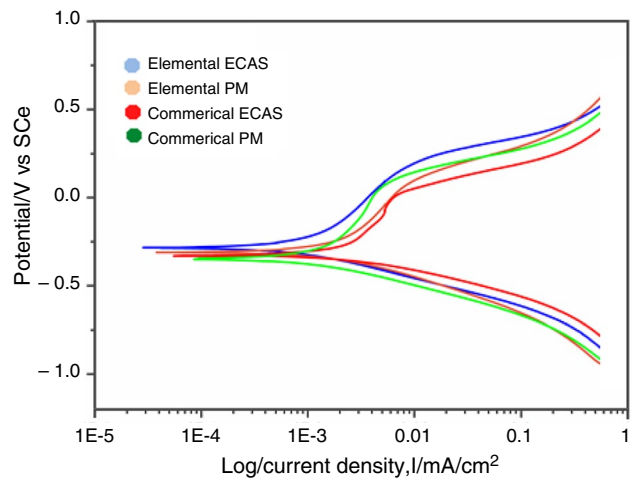
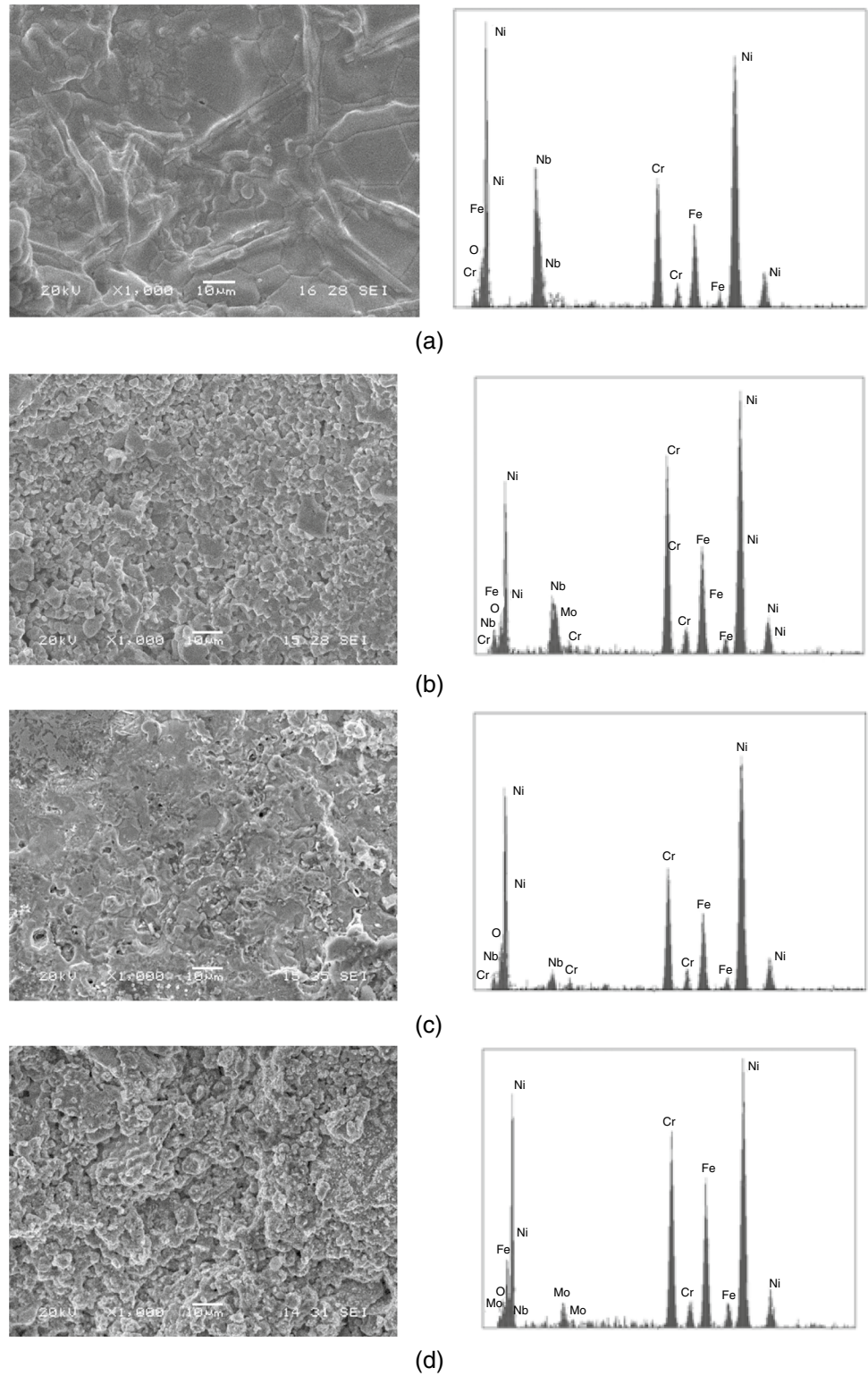


Fig. 20 Tafel curves of the samples in 3.5% NaCl solution after heat treatment

that the coated sample was 2.29 and the uncoated sample was $6.874\ g^2cm^{-4}s^2$. Electrochemical corrosion tests of the samples obtained by two different production methods using elemental powder mixture and commercial powder were carried out using three electrode technique in a solution medium of 3.5 mass% NaCl and 10 mass% $NaNO_3$ solution. Before the electrochemical corrosion experiments, the samples' open circuit potentials (OCP) against the reference electrode were determined after a waiting period of 1800s at a scanning speed of 5 mV/sec between -1 V and 1 V in order to stabilize the system. After OCP measurements, Tafel curves were obtained with $0.5\ mV\ s^{-1}$ scanning speed between -1 V and +1 V, I_{corr} , E_{corr} and corrosion rate were determined. The samples were obtained as a result of the production of Elemental Inconel 718 powder mixture by ECAS and PM methods and commercial In718 ready-made powders by ECAS and PM methods. Corrosion potentials in 3.5% NaCl solution were measured as -0.2838 mV, -0.3112 mV, -0.3306 mV and -0.3498 mV, respectively. Corrosion current densities due to these potentials were calculated

Fig. 21 SEM–EDS analyses of samples in 3.5 mass.% NaCl solution **a** elemental ECAS, **b** elemental PM, **c** commercial ECAS, **d** commercial PM



as 1.28 mA, 1.35 mA, 1.47 mA and 1.52 mA, respectively, using the Gamry device. The Tafel approach was applied in the calculations. The obtained corrosion value is given in Table 7. The closeness of the E_{corr} values obtained from the

Tafel curves to zero and the low current (I_{corr}) values mean that the corrosion resistance of the material is high.

In Fig. 20, it was seen that the sample prepared by using an elemental powder mixture and produced by the ECAS method had a higher corrosion potential and lower corrosion

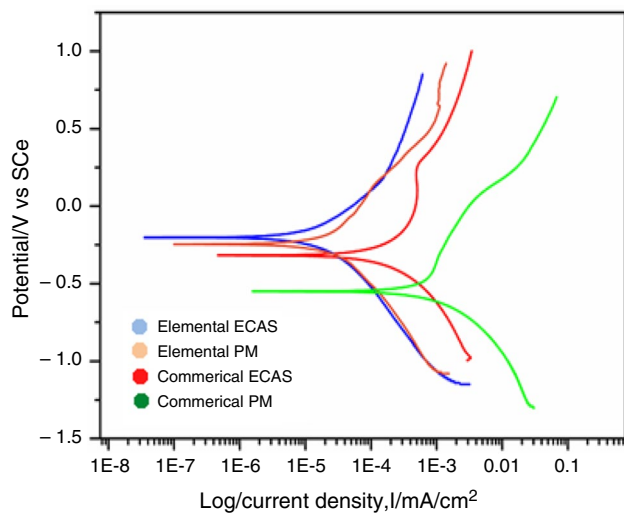


Fig. 22 Tafel curves of the samples in mass.% 10 NaNO₃ solution after heat treatment

Table 8 Tafel analysis results of samples in mass.%10 NaNO₃ solution

| Material | $I_{\text{corr}}/\text{A cm}^{-2}$ | E_{corr}/V | Corrosion rate/mpy |
|-----------------|------------------------------------|----------------------------|--------------------|
| Elemental ECAS | 0.93 | -0.188 | 10.56 |
| Elemental PM | 1.08 | -0.202 | 30.27 |
| Commercial ECAS | 1.41 | -0.246 | 70.31 |
| Commercial PM | 5.65 | -0.550 | 152.27 |

current density compared to the other samples, and the corrosion rate of this sample was lower than the other samples. In general, the samples produced with elemental powder mixture exhibit better corrosion resistance than those obtained with commercial powder, and it has been determined that the highest corrosion rate and therefore the lowest corrosion resistance are obtained in the commercial PM sample.

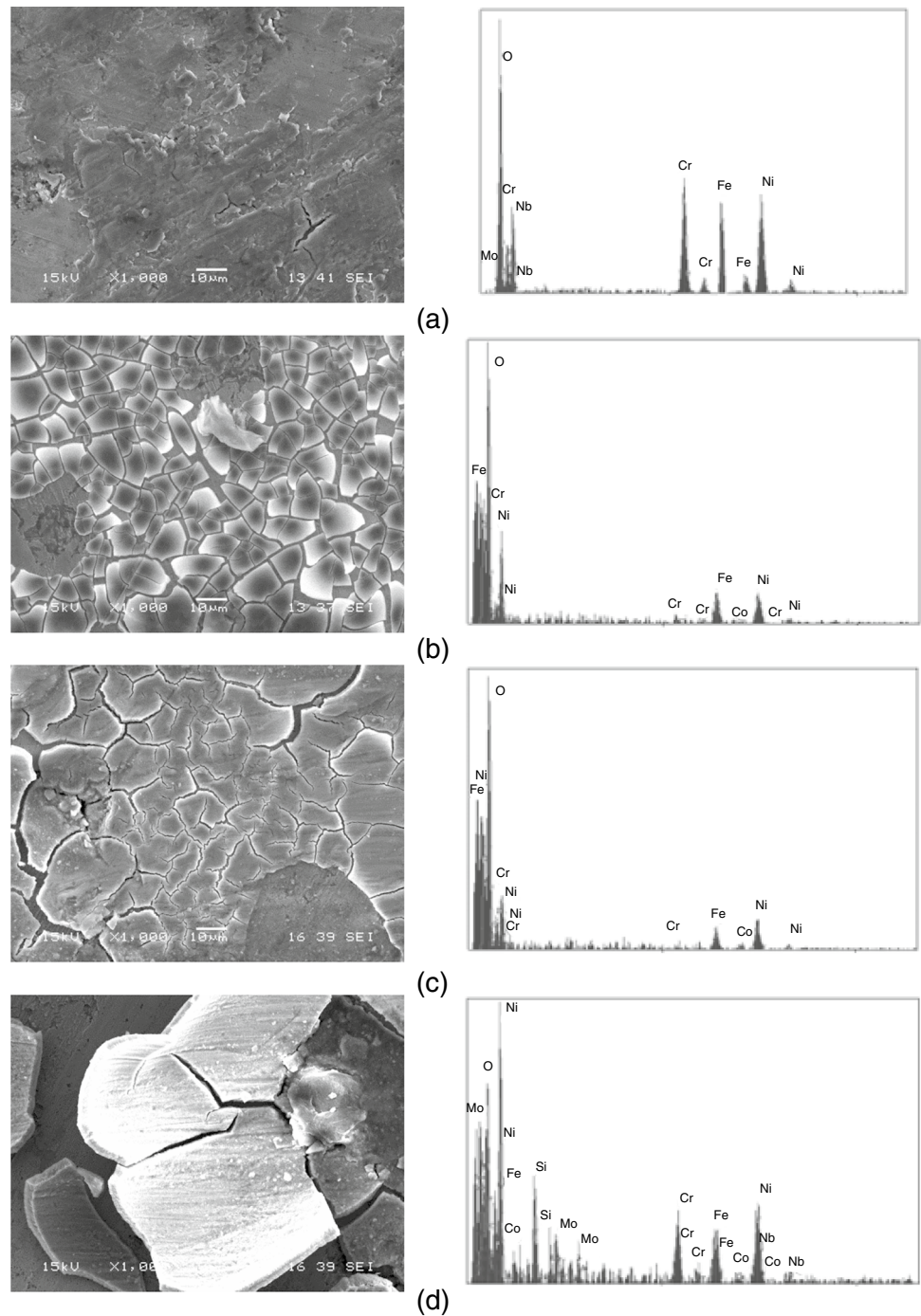
The microstructure changes and elemental analyses of the samples after the corrosion tests carried out in 3.5 mass% NaCl solution were carried out by SEM-EDS analysis examinations and are shown in Fig. 21a–d. It was observed that the samples produced by both methods using commercial powder were more corroded than those obtained with elemental powders. It was observed that elemental ECAS sample was less affected by corrosion by maintaining its surface integrity. When the samples are ranked from best to worst in terms of corrosion properties, it is seen from the EDS analyses taken from the samples that the amount of Nb decreases toward the worst sample.

Corrosion tests of the samples in mass %10 NaNO₃ solution were also carried out under similar conditions. Corrosion potentials of the samples obtained as a result of the production of elemental Inconel 718 powder mixture by ECAS and PM methods and Commercial In718 commercial powders by ECAS and PM methods were measured as -0.188 mV, -0.202 mV, -0.146 mV and -0.550 mV, respectively. Corrosion current densities due to these potentials were calculated as 0.93 mA, 1.08 mA, 1.41 mA and 5.56 mA, respectively, using the Gamry device. When the corrosion behavior of the samples in this solution environment is compared, it was determined that the sample exhibiting the best corrosion resistance was the elemental ECAS sample, as in all corrosive environments, as a result of the potential value being closer to zero and the corrosion current having a lower value. In Fig. 22, Tafel curves of the samples in 10% by mass NaNO₃ solution after heat treatment are given. In Table 8, Tafel analysis results of samples by mass are given in 10% NaNO₃ solution.

After the corrosion tests using mass.%10 NaNO₃ solution as the corrosive medium, the microstructure changes and elemental analyses of the samples were made by SEM-EDS analysis examinations and are shown in Fig. 23a–d. From the microstructural examinations, it was observed that the samples were corroded and a cracked corrosion layer was formed on their surfaces. It has been determined that the amount of corrosion products and cracks formed on the surface of the elemental ECAS sample is less than the others. From the EDS analyses of the samples, it was determined that a dense oxide layer of mass. % 50 was formed on the surfaces.

When the corrosion behavior of the samples in solutions was examined based on the electrochemical corrosion environments, it was observed that the samples other than the commercial PM sample gave better results in the NaNO₃ environment. While the corrosion rate of elemental ECAS sample is 45.59 mpy in NaCl environment, its rate is 10.56 mpy in NaNO₃ environment. While the corrosion rates of elemental PM and commercial ECAS samples, which exhibit similar properties, were 65.93 and 76.09 mpy in NaCl environment, respectively, the corrosion rates in NaNO₃ environment were determined as 30.27 mpy and 70.31 mpy, respectively. It is thought that the δ and Cr₂O₃ phases precipitated after the heat treatment are the reason why the sample, which was prepared using an elemental powder mixture and produced by the ECAS method, exhibited better corrosion behavior compared to the other samples. You et al. [38], in their study on Inconel 718 superalloy, emphasized that the γ' and γ'' phases affect the corrosion resistance negatively and the δ phase has the property of increasing the corrosion resistance.

Fig. 23 SEM–EDS analyses of samples in 10% mass.% NaNO_3 solution **a** elemental ECAS, **b** elemental PM, **c** commercial ECAS, **d** commercial PM



Conclusions

In this study, Inconel 718 powder mixtures obtained from the market as a commercial product and prepared from elemental powders were produced by conventional powder metallurgy (1300 °C/4 h) and electric current-assisted sintering (1700-2300A/10 min) methods. Then heat treatment consisting of a double-aging step was carried out. The following results were obtained from the characterization studies:

- The γ , δ , MC and C_2O_3 precipitate phase peaks defined in the literature were detected in the samples produced by both methods using elemental powders from XRD studies. However, the MC phase peak could not be detected in the production made with ECAS using commercial powder, and it was observed that the peak intensities of these precipitates were weakened in the sample produced with conventional PM.

- The relative densities of elemental ECAS, elemental PM, commercial ECAS and commercial PM samples were calculated as 98.96%, 98.46%, 97.94% and 97.63%, respectively. While the microhardness values of the produced samples were 245 ± 13 HV_{0.5}, 214 ± 17 HV_{0.5}, 208 ± 11 HV_{0.5} and 200 ± 6 HV_{0.5} before heat treatment, after heat treatment, it was determined as 344 ± 41 HV_{0.5}, 331 ± 32 HV_{0.5}, 314 ± 11 HV_{0.5} and 285 ± 17 HV_{0.5}.
- Corrosion behavior of samples isothermal hot corrosion in 40%Na₂SO₄ + 60%V₂O₅ salt environment at temperatures of 650, 750 and 850 °C for 1, 3, 5, 10, 20 and 30 h and 3.5 mass% NaCl and 10 mass% NaNO₃ solutions with the help of electrochemical corrosion tests. After electrochemical corrosion with 3.5 mass% NaCl solution, the corrosion rates of elemental ECAS, elemental PM, commercial ECAS and commercial PM samples were determined as 45.59 mpy, 65.93 mpy, 76.09 mpy and 77.82 mpy, respectively the corrosion rates in 10% mass% NaNO₃ solution were determined as 10.96 mpy, 30.27 mpy, 70.31 mpy and 152.27 mpy, respectively. Parabolic rate constant (k_p) values of these samples after hot corrosion are, respectively, 0.52, 1.06, 2.23 and 7.02 g²cm⁻⁴s² for 650 °C; 0.61, 2.47, 4.41 and 9.57 g²cm⁻⁴s² for 750 °C; and 0.93, 0.89, 0.95 and 0.99 g²cm⁻⁴s² for 850 °C.
- When the results were evaluated in general, it was determined that the samples produced with the ECAS technique using elemental powders had the best results.
- This material group is promising as stable high temperature building materials when produced with the ECAS technique. It is conceivable that performance behavior under service conditions can be improved with ceramic coatings similar to ZrO₂.

Author contributions Prof. Dr. Ozkan Ozdemir contributed to the interpretation of XRD results, interpretation of SEM–EDS results and formal control of the article. Dr. Nuri Ergin contributed to the interpretation of wear results, interpretation of corrosion results, writing and shape control of the article. Research Assistant Necati Koçak contributed to the production of materials, characterization of materials, writing and stylistic control of the article.

Funding Open access funding provided by the Scientific and Technological Research Council of Türkiye (TÜBİTAK). This work is not supported by any organization.

Declarations

Conflict of interest The authors declare that they have no known competing financial interests or personal relationships that could have appeared to influence the work reported in this paper.

Open Access This article is licensed under a Creative Commons Attribution 4.0 International License, which permits use, sharing,

adaptation, distribution and reproduction in any medium or format, as long as you give appropriate credit to the original author(s) and the source, provide a link to the Creative Commons licence, and indicate if changes were made. The images or other third party material in this article are included in the article's Creative Commons licence, unless indicated otherwise in a credit line to the material. If material is not included in the article's Creative Commons licence and your intended use is not permitted by statutory regulation or exceeds the permitted use, you will need to obtain permission directly from the copyright holder. To view a copy of this licence, visit <http://creativecommons.org/licenses/by/4.0/>.

References

1. Cho H, Lee DM, Lee JH, Bang KH, Lee BW. Thermal oxidation behavior of ceramic-coated Ni–Cr-base superalloys. *Surf Coat Technol.* 2008;202:5625–8.
2. Rao G, Kumar M, Srinivas M, Sarma DS. Effect of standart heat treatment on the microstructure and mechanical properties of hot isostatically pressed superalloy Inconel 718. *Mater Sci Eng.* 2003;A355:114–25.
3. Gülsoy HÖ, Özbek S, Günay V, Baykara T. Mechanical properties of powder injection molded Ni-based superalloys. *Adv Mater Res.* 2011;278:289–94.
4. Penkala HJ, Wosik J, Filemonowicz A. Quantitative microstructural characterization of Ni-base superalloys. *Mater Chem Phys.* 2003;81:417–23.
5. Chen YC, Liao YS. Study on wear mechanisms in drilling of inconel 718 superalloy. *J Mater Process Technol.* 2003;140:269–73.
6. Alniak MO, Bedir F. Hot forging behavior of Nickel based superalloys under elevated temperatures. *Mater Design.* 2010;31:1588–92.
7. Kasim MS, Haron CH, Ghani JA, Sulaiman MA, Yazid MZA. Wear mechanism and notch wear location prediction model in ball nose end milling of inconel 718. *Wear.* 2013;302:1171–9.
8. Rao GA, Srinivas M, Sarma DS. Effect of thermomechanical working on the microstructure and mechanical properties of hot isostatically pressed superalloy Inconel 718. *Mater Sci Eng.* 2004;A383:201–12.
9. Ergin N, Özdemir Ö. An investigation on TiNi intermetallic produced by electric current activated sintering. *Acta Physica Polonica A.* 2012;123:248–9.
10. Orru R, Licheri R, Locci AM, Cincotti A, Cao G. Consolidation/synthesis of materials by electric current activated/assisted sintering. *Mater Sci Eng.* 2009;R63:127–87.
11. Grasso S, Sakka Y, Marzza G. Electric current activated/assisted sintering (ECAS): a review of patents 1906–2008. *Sci Technol Adv Mater.* 2009;10:1–24.
12. Marshall K, Schillinger P, Weston NS, Epler M, Jackson M. A parametric study of the microstructural evolution of an advanced Ni-based superalloy powder when consolidated using Field Assisted Sintering Technology, compared to a hot isostatic pressing benchmark. *Adv Ind Manuf Eng.* 2022;5: 100103.
13. Ma LY, Wan M, Zhang ZY, Meng B. Effect of sintering duration on microstructure and properties of Inconel 718 superalloy prepared by electric field-activated sintering. *J Manuf Process.* 2023;105:27–37.
14. Yan S, Wang Q, Chen X, Zhang C, Cui G. Fabrication of highly compact Inconel 718 alloy by spark plasma sintering and solution treatment followed by aging. *Vacuum.* 2019;163:194–203.

15. Stopka KS, Desrosiers A, Nicodemus T, Krutz N, Andreaco A, Sangid MD. Intentionally seeding pores in additively manufactured alloy 718: Process parameters, microstructure, defects, and fatigue. *Addit Manuf.* 2023;66: 103450.
16. Faheem M, McCormick S, Chant I. Microstructural and DSC studies of Alloy 718 plus. *Thermochim Acta.* 2009;496:151–5.
17. Mei Y, Liu Y, Liu C, Li C, Yu L, Guo Q, Li H. Effect of cold rolling on the precipitation kinetics and the morphology evolution of intermediate phases in Inconel 718 alloy. *J Alloys Compd.* 2015;649:949–60.
18. Voort GFV, Manilova EP, Lucas GM. Metallographic techniques for superalloys. *Microsc Microanal.* 2004;10:1–22.
19. Zhu L, Xu ZF, Liu P, Gu YF. Effect of processing parameters on microstructure of laser solid forming Inconel 718 superalloy. *Opt Laser Technol.* 2018;98:409–15.
20. Liu WC, Yao M, Chen ZL, Wang SG. Niobium segregation in Inconel 718. *J Mater Sci.* 1999;34:2583–6.
21. Wang C, Li R. Effect of double aging treatment on structure in Inconel 718 alloy. *J Mater Sci.* 2004;39:2593–5.
22. Li RB, Yao M, Liu WC, He XC. Isolation and determination for δ , γ' and γ'' phases in Inconel 718 alloy. *Scripta Mater.* 2002;46:635–8.
23. Rai SK, Kumar A, Shankar V, Jayakumar T, Rao KBS, Raj B. Characterization of microstructures in Inconel 625 using X-ray diffraction peak broadening and lattice parameter measurements. *Scripta Mater.* 2004;51:59–63.
24. Sundararaman M, Mukhopadhyay P, Banerjee S. Carbide precipitation in Nickel base superalloys 718 and 625 and their effect on mechanical properties. *Miner Metals Mater Soc.* 1977. https://doi.org/10.7449/1997/superalloys_1997_367_378.
25. Delaunay F, Berthier C, Lenglet M, Lameille JM. SEM-EDS and XPS studies of the high-temperature oxidation behaviour of Inconel 718. *Mikrochim Acta.* 2000;132:337–43.
26. Candioto KCG, Calari FR, Reis DAP, Couto AA, Nunes CA. Mechanical and materials engineering of modern structure and component design. In: Öchsner A, Altenbach H, editors. *Characterization of the superalloy Inconel 718 after double aging heat treatment. Advanced Structured Materials*, vol. 70. Cham: Springer; 2015. p. 293–300.
27. Lia F, Park JZ, Keist JS, Joshi S, Martukanitz RP. Thermal and microstructural analysis of laser-based directed energy deposition for Ti–6Al–4V and Inconel 625 deposits. *Mater Sci Eng.* 2018;A717:1–10.
28. Park JM, Ryu WS, Kang YH. DSC study on carbide precipitation reaction in Inconel 600. *J Nuclear Mater.* 1994;209:221–5.
29. Zauner R, Heaney D, Piemme J, Binet C, German R. The effect of powder type and powder size on dimensional variability in PIM. In: *PM2Tec2002 world congress on powder metallurgy and particulate materials 2002*;191–98
30. Qin H, Bi Z, Yu H, Feng G, Du J, Zhang J. Influence of stress on γ'' precipitation behavior in Inconel 718 during aging. *J Alloys Compd.* 2018;740:997–1006.
31. Tucho WM, Cuvillier P, Atle SK, Hansen V. Microstructure and hardness studies of Inconel 718 manufactured by selective laser melting before and after solution heat treatment. *Mater Sci Eng.* 2017;A689:220–32.
32. Schafrik, R.E.; Ward, D.D.; Groh, J.R. Application of Alloy 718 in GE Aircraft Engines: Past, Present and Next Five Years. In *Proceedings of the International Symposium on Superalloys and Various Derivatives*, Pittsburgh, PA, USA 2001; pp. 1–11.
33. Sequera A, Guo YB. Uncertainty analysis of tool wear and surface roughness in end milling. In: *Proceedings of the ASME 2013 international manufacturing science and engineering conference MSEC2013 2013*;1–7. USA
34. Kamal S, Sharma KV, Abdul-Ram AM. Hot corrosion behavior of superalloy in different corrosive environments. *J Miner Mater Charact Eng.* 2015;03:26–36.
35. Eliaz N, Shemesh G, Latanision RM. Hot corrosion in gas turbine components. *Eng Fail Anal.* 2002;9:31–43.
36. Azarmehr SA, Shirvani K, Schutze M, Galetz M. Microstructural evolution of silicon-platinum modified aluminide coatings on superalloy GTD-111. *Surface Coat Technol.* 2017;321:455–63.
37. Kamal S, Jayaganthan R, Prakash S, Kumar S. Hot corrosion behavior of detonation gun sprayed Cr_3C_2 –NiCr coatings on Ni and Fe-based superalloys in Na_2SO_4 –60% V_2O_5 environment at 900°C. *J Alloys Compd.* 2008;463:358–72.
38. You X, Tan Y, Zhao L, You Q, Wang Y, Ye F. Effect of solution heat treatment on microstructure and electrochemical behavior of electron beam smelted Inconel 718 superalloy. *J Alloys Compd.* 2018;741:792–803.

Publisher's Note Springer Nature remains neutral with regard to jurisdictional claims in published maps and institutional affiliations.